COMPUTATIONAL COMBUSTION 2007, ECCOMAS Thematic Conference
D. Roekaerts, P. Coelho, B.J. Boersma, K. Claramunt (Eds.)
18-20 July 2007, Delft, The Netherlands

DIRECT NUMERICAL SIMULATION OF TURBULENT LIFTED HYDROGEN/AIR JET FLAME IN AN AUTOIGNITIVE HEATED COFLOW

Chun S. Yoo[*], Jacqueline H. Chen[*], and Ramanan Sankaran[†]

*Combustion Research Facility,
Sandia National Laboratories, Livermore, CA 94551-0969, USA
E-mail: csyoo@sandia.gov; jhchen@sandia.gov

[†]National Center for Computational Sciences,
Oak Ridge National Laboratories, Oak Ridge, TN 37831-6008, USA
E-mail: sankaranr@ornl.gov

Key words: DNS, Lifted flame, Stabilization, Turbulent, Auto-ignition

Abstract. *Direct numerical simulation of the near field of a three-dimensional spatially developing turbulent slot-burner lifted jet flame in heated coflow is performed with a detailed hydrogen-air mechanism and mixture averaged transport properties at a jet Reynolds number of 11,000 with over 900 million grid points. The results show that auto-ignition in a fuel-lean mixture immediately upstream of the flame base is the main source of stabilization of the lifted jet flame and that HO_2 radical plays an important role in initiating and facilitating auto-ignition in both fuel-rich and fuel-lean mixtures. A Damköhler number analysis and intermediate species behavior near the leading edge of the lifted flame clearly show that auto-ignition occurs at the flame base. The flame index shows that both lean premixed and nonpremixed flame modes exist at the flame base, followed downstream by a prevailing premixed flame mode, and even further downstream, by the emergence of both rich premixed and nonpremixed flame modes. The DNS of the near field precludes the transition to a nonpremixed flame mode anticipated in the far-field of the jet. In addition to auto-ignition, vorticity generation due to baroclinic torque near the flame base assists in stabilizing the flame base by reducing the incoming local flow velocity, and thereby providing an environment enabling auto-ignition to proceed.*

1 INTRODUCTION

Turbulent lifted flames have been widely investigated due to their important role in practical applications such as direct injection stratified spark ignition engines, diesel engines and commercial boilers, and in understanding fundamental combustion phenomena as a building-block flame. In particular, the stabilization mechanism of a lifted flame base has

drawn great attention because the lifted flame base determines the overall flame stability and the characteristics of combustion systems[1–3]. Despite the importance of flame base stabilization, however, there has thus far been little consensus among researchers regarding the dominant mechanism which stabilizes the lifted flame base, not only because of the complex structure and propagation characteristics of turbulent lifted flames, but also because of the lack of three-dimensional measurement techniques for key scalar quantities together with the velocity field.

Several theories have been proposed to explain the stabilization mechanism of turbulent lifted jet flames, which can broadly be divided into two or three categories based on the premixedness of the mixture upstream of the flame base, or on the effect of local turbulent flow[1-3]. First, based on the degree of fuel-air premixing upstream of the flame base, the theories can be classified into three distinct categories: premixed flame theory, nonpremixed flamelet theory, and edge flame theory. In early experimental studies[4, 5], the mixture upstream of the lifted flame base is postulated to be premixed, and thus, the lifted flame is thought to stabilize where the relevant turbulent flame speed balances the local flow velocity. In the nonpremixed flamelet theory, it is proposed that combustion at the lifted flame base resembles an ensemble of laminar flamelets such that the flame can stabilize where the local scalar dissipation rate is below a critical value[6]. The edge flame theory, which combines elements of both premixed and nonpremixed flames, has been proposed[7, 8] since partially-premixed flames were experimentally reported[9] and found to play a critical role in stabilizing laminar nonpremixed jet flames[10]. According to the edge flame theory, the lifted flame base stabilizes where the edge flame propagation speed, which is two to three times larger than the laminar flame speed, matches the local flow velocity.

Second, stabilization theories can be categorized based on the effect of turbulent flow on the flame base – *i.e.* the turbulent intensity theory and large eddy concept. According to the turbulent intensity theory which is directly related to the premixed flame theory, turbulent intensity at the flame base enhances turbulent burning rates through flame area generation and flame propagation speed[8] and thus, a lifted flame can stabilize even at a position where the local flow velocity is considerably larger than the laminar flame velocity. The large eddy concept assumes that flame edge is able to propagate from one large eddy to another by moving along the flammable mixture, and thus, the flame edge stabilizes by oscillating with the passage of large eddy structures[11, 12].

The above theories are sometimes contradictory to one another, but sometimes complementary, depending upon the particular flames investigated. Recently, there have been attempts to explain the stabilization mechanism by combining several key elements from the theories[8, 12, 13]. However, definitive evidence substantiating the postulated mixed stabilization mechanisms is still unattainable due to inherent limitations in scalar-velocity measurements.

Recently, auto-ignition was proposed as another important stabilization mechanism of lifted flames in a heated coflow[14, 15]. Since auto-ignition can assist in stabilizing a turbulent flame base, the recirculation region of hot combustion products has been adopted in practical combustors. For example, in diesel engines, fuel is injected and mixed with a heated oxidizer coflow in the chamber at temperatures above the ignition limit, such that the stability and overall characteristics of the lifted flame and soot processes are highly affected by the heated

oxidizer stream[16].

In addition to the numerous experimental studies on flame stabilization, recently a few direct numerical simulations (DNS) of turbulent lifted jet flames have been performed[17–20]. In contrast to experiments in which only a few flame markers and the velocity field can be measured in two dimensions, DNS can provide full characterization of the flame structure and flow field near the flame base. Takeno and his coworkers introduced the concept of a flame index, the inner product of fuel and oxidizer gradients, to distinguish premixed flame zones from the prevailing nonpremixed flame in two-dimensional turbulent lifted jet flames[17]. Recently, stabilization characteristics of a lifted jet flame in a heated shear layer were investigated using a two-dimensional DNS with single-step global chemistry by Jiménez and Cuenot[18], in which re-ignition triggered by recirculated hot gas was found to be the key mechanism to stabilize the lifted triple flame along with large scale structures. While providing qualitative insights regarding the roles of auto-ignition and edge propagation, this study does not include realistic timescales associated with ignition kinetics relative to mixing time scales owing to the two-dimensional configuration and the simple chemistry. Mizobuchi et al.[19, 20] performed a three-dimensional DNS of a hydrogen lifted turbulent jet flame in an ambient coflow of oxidizer with detailed chemistry and identified the existence of nonpremixed flame islands. Their results support the premixed flame theory, primarily because the lift-off height is well correlated with the empirical equation proposed by Kalghatgi[5]. They did not, however, present detailed evidence to support the theory.

In the present study, the stabilization mechanism of a turbulent lifted hydrogen jet flame in a heated coflow is investigated by performing three-dimensional DNS with detailed hydrogen/air chemistry. While this is the first three dimensional DNS with detailed chemistry performed of this configuration, there have been transported probability density function (PDF) methods applied to the experimental Cabra burner[14, 21-24], in which the lift-off height is predicted with reasonable accuracy. These models also show that the lift-off height is sensitive to a recombination reaction, $H + O_2 + M \rightarrow HO_2 + M$ and that HO_2 exists upstream of other intermediate species. These results suggest that auto-ignition occurs at the flame base. Thus, in the present DNS study the role of auto-ignition resulting from the heated coflow is examined in detail to determine the stabilization mechanism of the flame. In addition, the flame structure is characterized at different axial locations along with the conditional flame statistics. Finally, the instantaneous and time-averaged flow field in the vicinity of the flame base is characterized and its role in stabilization elucidated.

2 PROBLEM CONFIGURATION

The simulation was performed in a three-dimensional slot-burner configuration. Fuel issues from a central jet, which consists of 65% hydrogen and 35% nitrogen by volume with an inlet temperature of 400K. The central jet is surrounded on either side by co-flowing heated air at 1100 K. This temperature is greater than the crossover temperature of hydrogen-air chemistry[25], such that the mixture upstream of the flame base is auto-ignitable.

The simulation parameters are given in Table 1. A uniform grid spacing of 15μm was used in the streamwise direction, x, and spanwise direction, z, while an algebraically stretched mesh

Parameter	
Slot width (h)	1.92mm
Domain size in the streamwise, transverse and spanwise directions ($L_x \times L_y \times L_z$)	$12.5h \times 16.7h \times 3.3h$
Number of grid points	$1600 \times 1372 \times 430 \approx 944$ M
Turbulent jet velocity (U)	347.0m/s
Laminar coflow velocity	4.0m/s
Jet Reynolds number ($\mathrm{Re}_{\mathrm{jet}} = Uh/\nu$)	11200
Turbulent intensity‡ (u'/U)	0.087
Turbulent length scale‡, § (l_t/h)	0.78
Turbulent Reynolds number‡ ($\mathrm{Re}_t = u' l_t/\nu$)	360

Table 1 : Numerical and physical parameters of the DNS

was used in the transverse direction, y, obtained from $y(s) = f(s) \times s$, where s is the equi-spaced computational grid and $0 \le s \le 1$. The stretching function is given by,

$$f(s) = \beta s + \frac{1}{2}\left(1 + \tanh\frac{s - s^*}{\sigma}\right)\left(e^{ks} - \beta s\right) \tag{1}$$

where $k = \ln(s^*)/(s^*-1)$, $\beta = 0.64$, $s^* = 0.80$, and $\sigma = 1/20$. To obtain a symmetric mesh, the mesh was mirrored across the jet centerline ($y = s = 0$). The resultant mesh provides a uniform grid spacing of 15 μm over a $8h$ wide region in the center of the domain. Details of the mesh structure are given in Sankaran et al.[26]

The compressible Navier-Stokes, species continuity, and total energy equations were solved using the Sandia DNS code, S3D. A fourth-order explicit Runge-Kutta method for time integration and an eighth-order central spatial differencing scheme were used with a tenth-order filter to remove any spurious high frequency fluctuations in the solutions[27, 28]. A detailed hydrogen-air kinetic mechanism[29] was used, and CHEMKIN and TRANSPORT software libraries[30, 31] were linked with S3D to evaluate reaction rates, thermodynamic and mixture-averaged transport properties.

Navier-Stokes characteristic boundary conditions (NSCBC) were used to prescribe the boundary conditions. Nonreflecting inflow/outflow boundary conditions[32, 33] were used in the streamwise and transverse directions and periodic boundary conditions were applied in the homogeneous spanwise direction. Based on the prescribed inlet jet velocity and the streamwise domain length, a flow-through time is approximately 0.7ms. The solution was advanced at a constant 4ns time-step through 7.5 flow-through times to provide stationary statistics. The simulation was performed on the 50 Tflop Cray XT3 at Oak Ridge National Laboratories and required 2.5 million CPU-hours running for 10 days on 10,000 processors.

‡ u', l_t, and ν are evaluated at the 1/4th streamwise location along the jet centerline

§ Turbulence length scale l_t is estimated as $l_t = u'^3/\varepsilon$, where ε is the averaged turbulent kinetic energy dissipation rate.

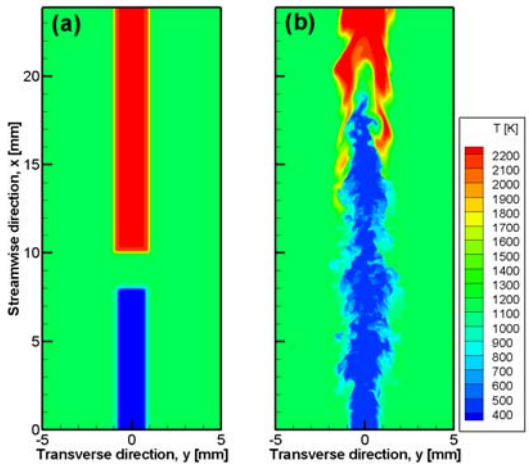

Figure 1: Temperature isocontours in the plane, $z = 0$, at (a) $t = 0.0$ and (b) 0.03 ms.

To facilitate the simulation, the central hydrogen/nitrogen jet is ignited by artificially imposing a high temperature region in the central jet as shown in Fig. 1 (a). The initial hot region is readily swept out of the domain by the fast central jet within one flow-through time as shown in Fig. 1(b). After five flow-through times, the lifted jet flame base fluctuates about its steady stabilization lift-off height of approximately $x = 7.5$mm.

3 RESULTS AND DISCUSSION

The global structure of the flame stabilization base is revealed from instantaneous images of the flame structure at different times. Figure 2 shows the instantaneous isocontours of the mass fraction of hydroxyl (Y_{OH}), which is often used as an experimental marker of the lifted flame base[11, 34], superimposed on the iso-surface of stoichiometric mixture fraction, ($\xi_{st} = 0.199$) at $t = 0.42$ms (approximately six flow-through times). The mixture fraction is computed using Bilger's formula[35] based on the elemental mass fractions of the fuel and oxidizer. At first glance, one can see that fine flow structures upstream of the flame base are readily dissipated as the flow traverses downstream, primarily due to the effect of heat release by the flame[36]. In addition, the flame base is highly irregular and strongly affected by the instantaneous local flow and mixture conditions such that the stabilization of the lifted jet flame is not a global phenomenon, but rather, a highly localized phenomenon.

Although three-dimensional volume rendering provides a description of global features pertaining to the flame structure, they are too complex to extract details regarding the lifted flame. Instead, instantaneous snapshots of a two-dimensional x-y plane are extracted from the three-dimensional data. Figure 3 shows the isocontours of temperature, heat release rate, OH and HO_2 mass fractions on the $z = 0$ plane at $t = 0.42$ms. One can readily observe that the flame base stabilizes in a fuel-lean mixture rather than at the stoichiometric mixture, which is insensitive to the definition of the flame base. Moreover, it is clear that HO_2 radical accumulates upstream of OH and other high-temperature radicals such as H and O which are not shown here. HO_2 radical is a precursor of auto-ignition in hydrogen/air chemistry [23, 37] so

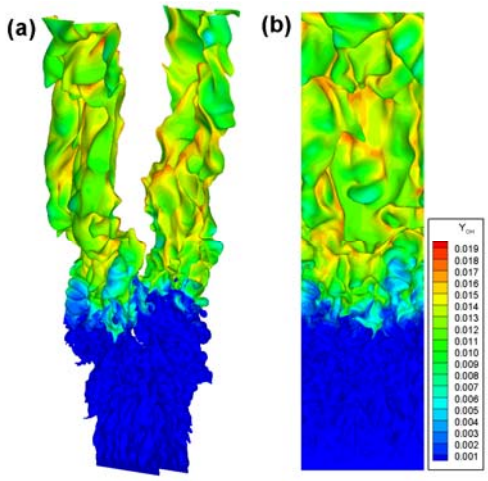

Figure 2: Isocontours of the mass fraction of hydroxyl radical (OH) superimposed on the iso-surface of stoichiometric mixture fraction (ξ_{st} = 0.199) at 0.42ms; (b) is another image of (a) viewed from the spanwise direction, z.

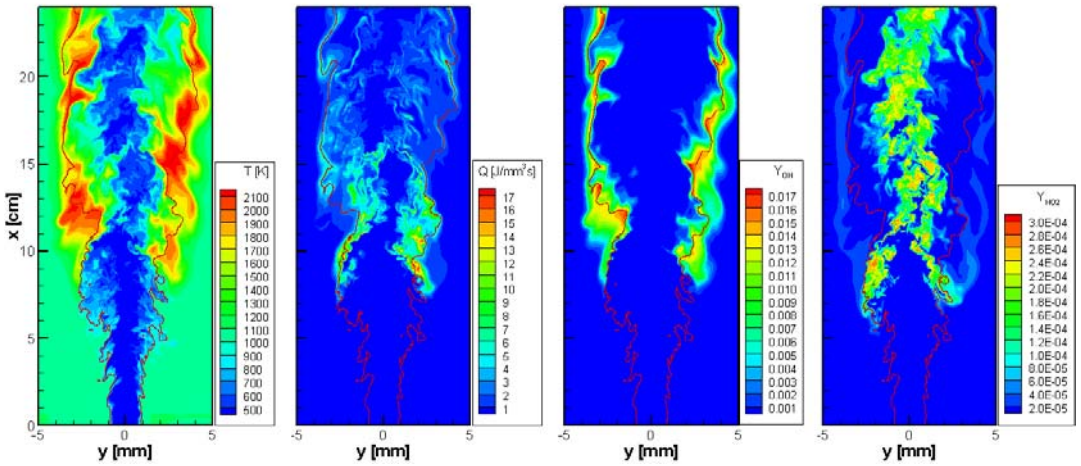

Figure 3: From left to right, isocontours of temperature, heat release rate, Y_{OH} and Y_{HO2} in the plane z = 0 at t = 0.42ms. The solid red line denotes the stoichiometric mixture fraction.

that the existence of HO_2 radical upstream of other intermediate radicals indicates that the stabilization mechanism of the lifted flame base is due to auto-ignition by heated coflow rather than normal flame propagation[23].

In the following sections, details of the lifted flame stabilization mechanism will be presented in terms of the instantaneous flame and flow structures at different axial and spanwise locations in the jet, along with averaged and conditional mean flame statistics.

3.1 Ignition/extinction processes at the flame base

To understand in detail what happens near the flame base, we investigate the temporal evolution of the flame and flow characteristics at the flame base. Figure 4 shows a typical

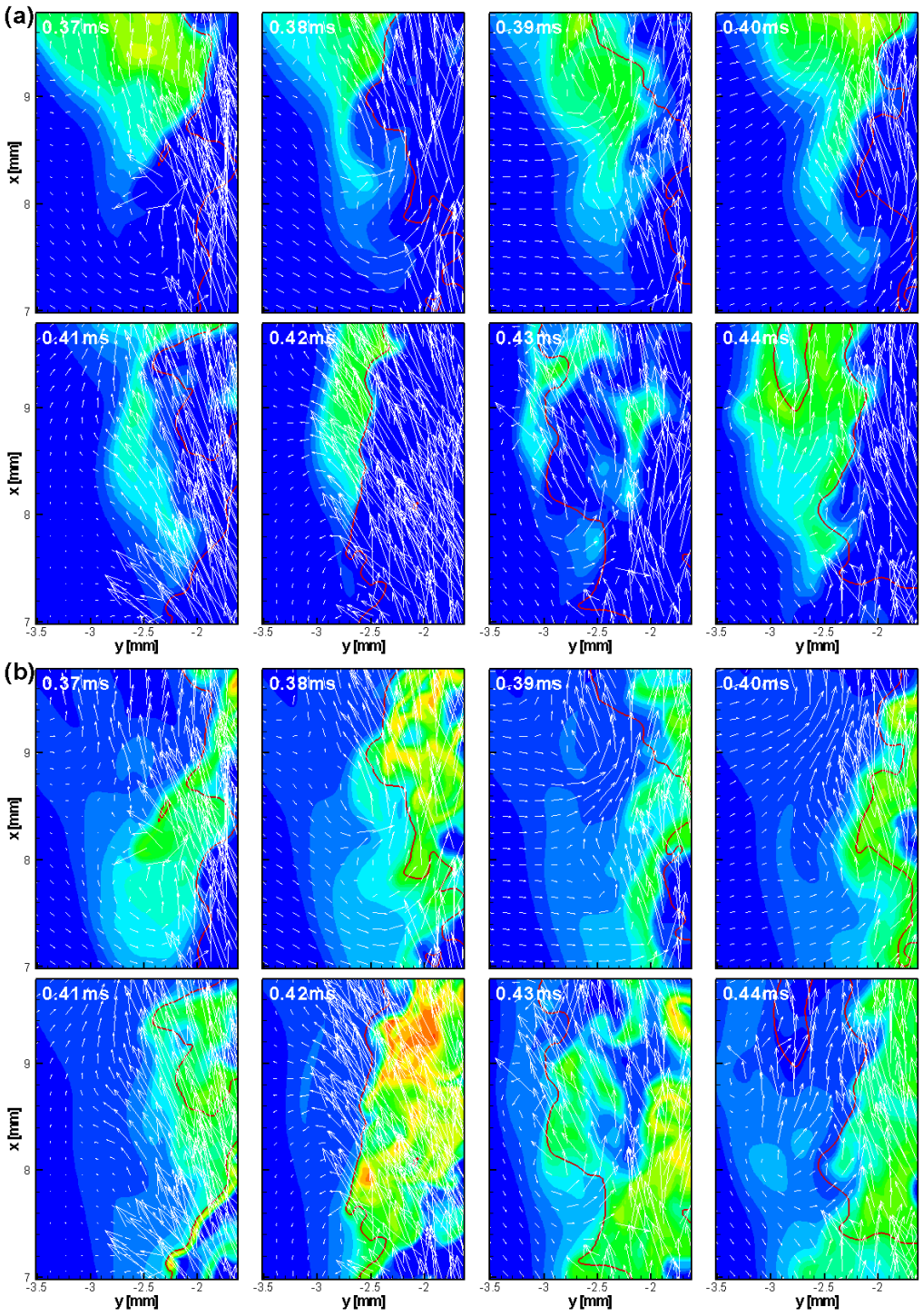

Figure 4: Sequential images of (a) Y_{OH} and (b) Y_{HO2} isocontours (color flood) at the leading edge of the lifted flame with velocity field (white arrowed line) and stoichiometric mixture fraction line (solid red line) from t = 0.37 to 0.44ms in 0.01ms increments.

sequence of images of Y_{OH} and Y_{HO2} isocontours at the leading edge of the lifted jet flame between t = 0.37 and 0.44ms. As mentioned before, OH is a good marker of the high-temperature flame zone, whereas HO_2 is a good marker of ignition upstream of the flame base. Also shown in the figure are the stoichiometric mixture fraction isoline and the instantaneous velocity vectors. Note that the leading edge shown here corresponds to the left branch of the lifted flame, and hence, the centerline of the fuel jet lies to the right side of each figure (not shown in the figures). Several important characteristics of the lifted flame are deduced from this and many other image sequences. First, the flame base moves upstream following a fuel-lean mixture, and not the stoichiometric mixture fraction as previously mentioned. Second, while moving upstream (e.g. between 0.37 and 0.40ms), the flame base is convected by a positive spanwise vortex ($\omega_z > 0$) which helps to stabilize the base and/or assist in its propagation. Third, it is readily observed that a pool of HO_2 exists ahead of the OH radical which enhances the movement of the ignition front upstream.

After 0.40ms, a region with high scalar dissipation rate, χ (in excess of 10,000s^{-1}, which is close to the extinction scalar dissipation rate, χ_q of the corresponding strained laminar nonpremixed flame) advects toward the flame base and extinguishes the flame at t = 0.42ms. The scalar dissipation rate is defined by[3, 37]:

$$\chi = 2\alpha\left|\nabla\xi\right|^2, \tag{2}$$

where α is the thermal diffusivity. However, this region also generates a high level of HO_2 via the recombination reaction, $H + O_2 + M \rightarrow HO_2 + M$ (R9) so that re-ignition occurs immediately following extinction and HO_2 generation not only in fuel-lean mixtures but also in fuel-rich mixtures (see figures at t = 0.43ms). Therefore, one can observe that this re-ignition region is demarcated by a depletion in HO_2 coincident with an increase in OH by comparing Figs. 4 (a) and (b) at t = 0.43ms.

We also identify another interesting ignition process occurring on the right branch of the lifted flame. Figure 5 shows sequential images of Y_{OH} and Y_{HO2} isocontours on the right branch at the leading edge of the lifted jet flame between t = 0.37 and 0.44ms. In this case, one can find a negative vortex ($\omega_z < 0$) which helps to stabilize the flame base similar to the left branch of the lifted flame in Fig. 4. Also notable is an ignition process occurring in a fuel-rich mixture island. At t = 0.37ms, note that there is a rich mixture island in the two-dimensional plane corresponding to a three-dimensional structure, *i.e.* a rich mixture arm emanating from the homogeneous spanwise direction, z. The island contains a high concentration of HO_2, and thus its presence initiates auto-ignition. A few hundredths of a millisecond later, HO_2 induces auto-ignition which results in the increase of OH observed in Fig. 5(a). This result clearly shows that HO_2, which is generated in the cold fuel jet and advected to the hot oxidizer region by local turbulent flow, facilitates ignition in the fuel-lean mixture. Note that this ignition pattern would not occur in two-dimensional simulations because the rich mixture island originates from the out-of-plane homogeneous direction.

To determine whether similar flame characteristics obtained from instantaneous realizations exist from an averaged point of view, the three-dimensional data is Favre averaged over time and the homogeneous direction, z. Figure 6 shows isocontours of

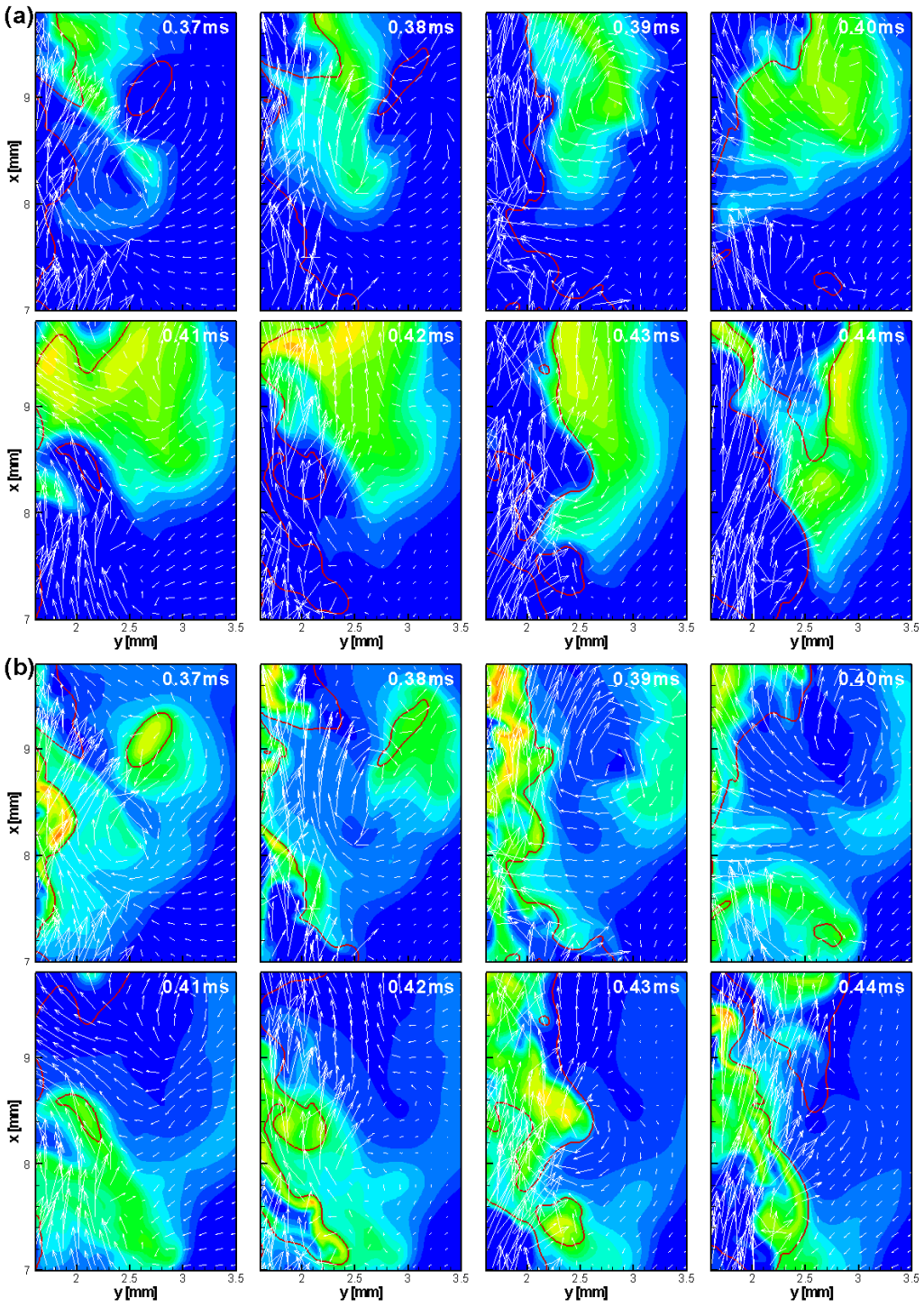

Figure 5: Sequential images of (a) Y_{OH} and (b) Y_{HO2} isocontours (color flood) at the leading edge of the lifted flame with velocity field (white arrowed line) and stoichiometric mixture fraction line (solid red line) from t = 0.37 to 0.44ms in 0.01ms increments.

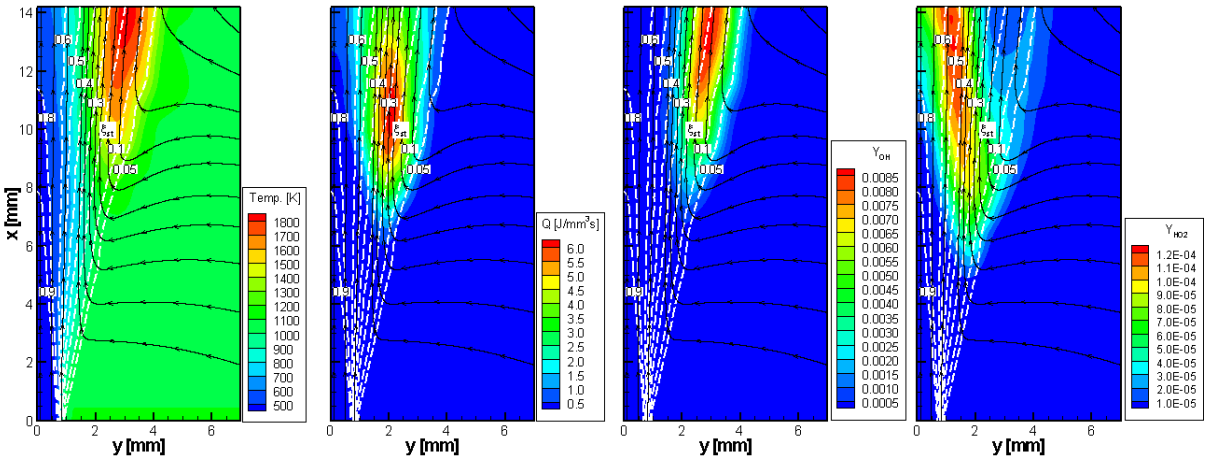

Figure 6: Isocontours of Favre averaged temperature, heat release rate, Y_{OH} and Y_{HO2} with mixture fraction lines (dashed white line) and streamlines (arrowed black line). All values are averaged over a time period between 0.28 to 0.51ms and the homogeneous direction, z.

averaged temperature, heat release rate, Y_{OH} and Y_{HO2} along with mixture fraction isolines and streamlines. As in the instantaneous realizations shown above, the average values also show that the flame base lies in a fuel-lean mixture (*i.e.* $\xi \approx 0.1$) and that HO_2 is concentrated upstream of OH. In addition, near the flame base, the streamlines reflect flow redirection which further helps to stabilize the flame base.

From these results, we conclude that auto-ignition in a fuel-lean mixture at the flame base is the primary method of flame stabilization, and that HO_2 radicals play a critical role in initiating and facilitating the ignition process. Occasionally, auto-ignition in a fuel rich mixture can also occur near the flame base immediately after flame extinction by high scalar dissipation rate, although the probability of occurrence of ignition in fuel rich mixtures is much lower than in fuel lean mixtures. Finally, spanwise vortices near the flame base act to reduce the incoming axial core jet velocity, providing additional shelter for the ignition process.

3.2 Flame structure and flame index

To better understand the flame characteristics at different downstream locations, we examine the flame structure and flame index which is often used to discern premixed flame zones from the prevailing nonpremixed flame in lifted jet flames. The flame index is defined by[17]:

$$F.I. = \nabla Y_F \cdot \nabla Y_O \,, \tag{3}$$

where the subscripts F and O represent fuel and oxidizer, respectively.

Figure 7 shows isocontours of heat release rate with the stoichiometric mixture fraction isoline at several axial locations in the jet flame. The flame index is also superimposed in the figure to distinguish between premixed and nonpremixed flame modes. Near the flame base (x = 7.5mm), the main heat release rate occurs in a fuel-lean mixture, but reactants seem to

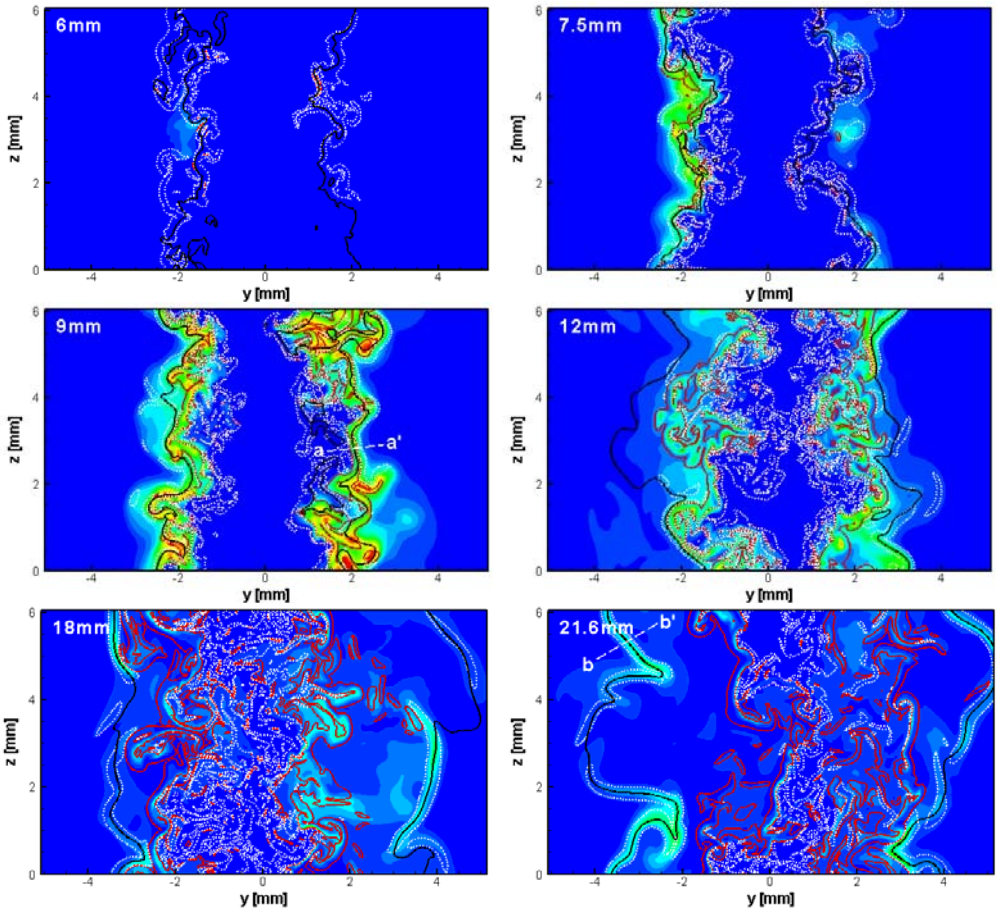

Figure 7: Isocontours of heat release rate with stoichiometric mixture fraction line (solid black line) for different axial, x, locations; 6, 7.5, 9, 12, 18, and 21.6mm. The solid red line and dotted white line represent the flame index = 0.005/mm^2 and -0.005/mm^2, which represent premixed and nonpremixed flame regions, respectively

burn in both premixed and nonpremixed flame modes. At x = 9mm, although heat release rate occurs near the stoichiometric mixture, reaction occurs primarily in a premixed flame mode. At x = 12mm, the heat release rate has migrated toward much richer mixtures, and reaction occurs primarily in a rich premixed flame mode. Further downstream (at x = 18 and 21.6mm), however, heat release rate occurs in both fuel-rich and stoichiometric mixtures. In these regions, the premixed flame mode prevails in fuel-rich mixtures, whereas near stoichiometric conditions nonpremixed flame mode prevails. By examining the flame index, it is readily observed that auto-ignition does not show any bias towards a particular combustion mode at the leading part of the lifted flame. It is not until further downstream that the normal nonpremixed and fuel-rich premixed flames develop further. Note also that the transition to a fully nonpremixed flame in the absence of a premixed flame mode is not found in the present simulation, where the domain size encompasses only the near field of the jet. Therefore, at the downstream boundary of the domain the core fuel jet still exists and thus, fuel-rich premixed flames are also sustained by the core jet.

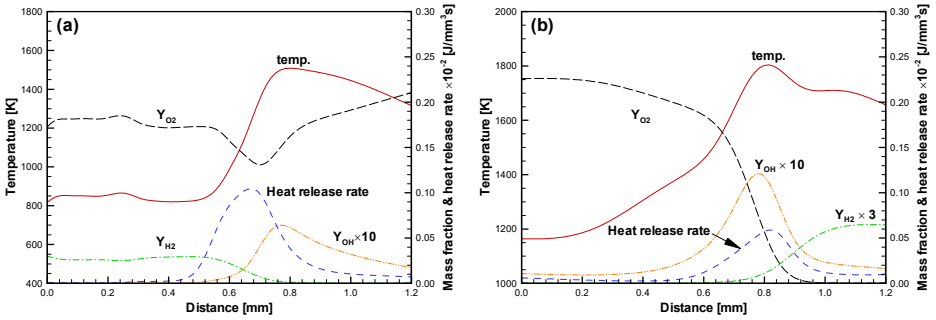

Figure 8: Flame structures along the 1D lines in Fig.7; (a) a-a' at 9mm and (b) b-b' at 21.6mm.

The detailed flame structure associated with the premixed and nonpremixed flame modes is obtained by examining several representative cuts from Fig. 7. Figure 8 shows the flame structures along the cuts (a-a' at 9mm and b-b' at 21.6mm) from Fig. 7. Typical premixed and nonpremixed flame structures are clearly identified in Fig. 8 (a) and (b), respectively. In the premixed flame, fuel and oxidizer diffuse into the reaction zone from the same direction, whereas in the nonpremixed flame, they approach the reaction zone from opposite directions.

3.3 Statistics on flame characteristics

In this section, conditional flame statistics are presented to further elucidate the stabilization mechanism and flame structure, and also to provide useful information for model development and validation. Figure 9 shows scatter plots of temperature versus mixture fraction at different axial locations at t = 0.42ms. Open circles and diamonds represent, respectively, the conditional mean and standard deviation of temperature. The frozen

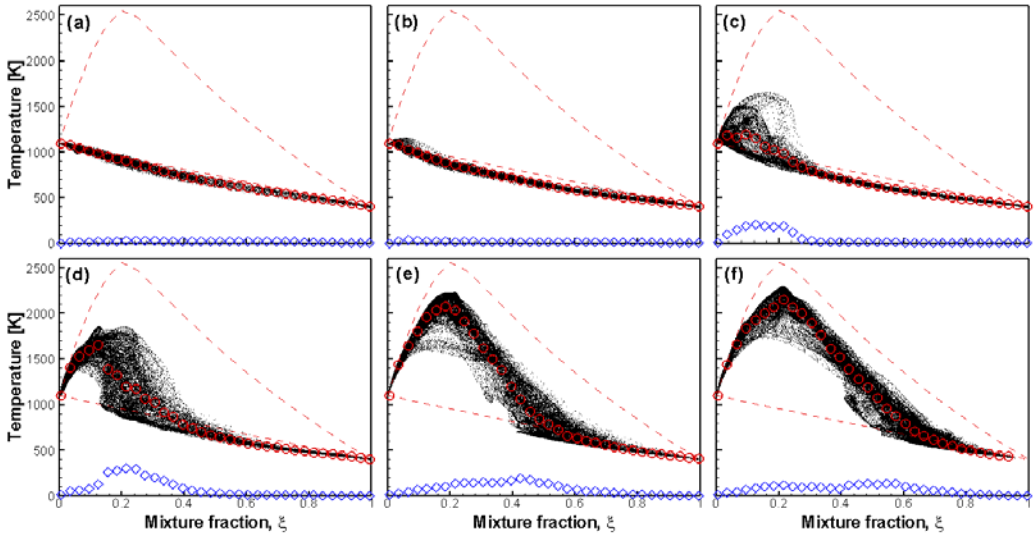

Figure 9: Scatter plots of temperature versus mixture fraction for different axial locations; from (a) to (f), x = 2.4, 6, 7.5, 9, 12, and 18 mm. Dashed lines denote inflow and equilibrium temperatures, and open circles and diamonds denote respectively the conditional mean and standard deviation of temperature.

inflow and equilibrium temperature are also represented by dashed lines. At first glance, one can observe that upstream of the flame base, the temperature profile deviates from the inflow condition as shown in Figs. 9 (a) and (b). Due to differential diffusion, hydrogen in the cold fuel jet diffuses into the hot oxidizer faster than other species, and hence, pure mixing of the reactants results in a temperature deficit through the entire mixture space relative to the inflow temperature. This temperature drop becomes more significant at downstream axial positions. Note also that temperature first increases in a fuel-lean mixture, and subsequently the peak shifts towards richer mixtures, clearly indicating that ignition occurs first under hot, lean conditions where ignition delays are shorter. This has also been demonstrated in previous two-dimensional DNS of auto-ignition in an inhomogeneous hydrogen/air mixture (see Fig. 9 in Echekki and Chen[37]).

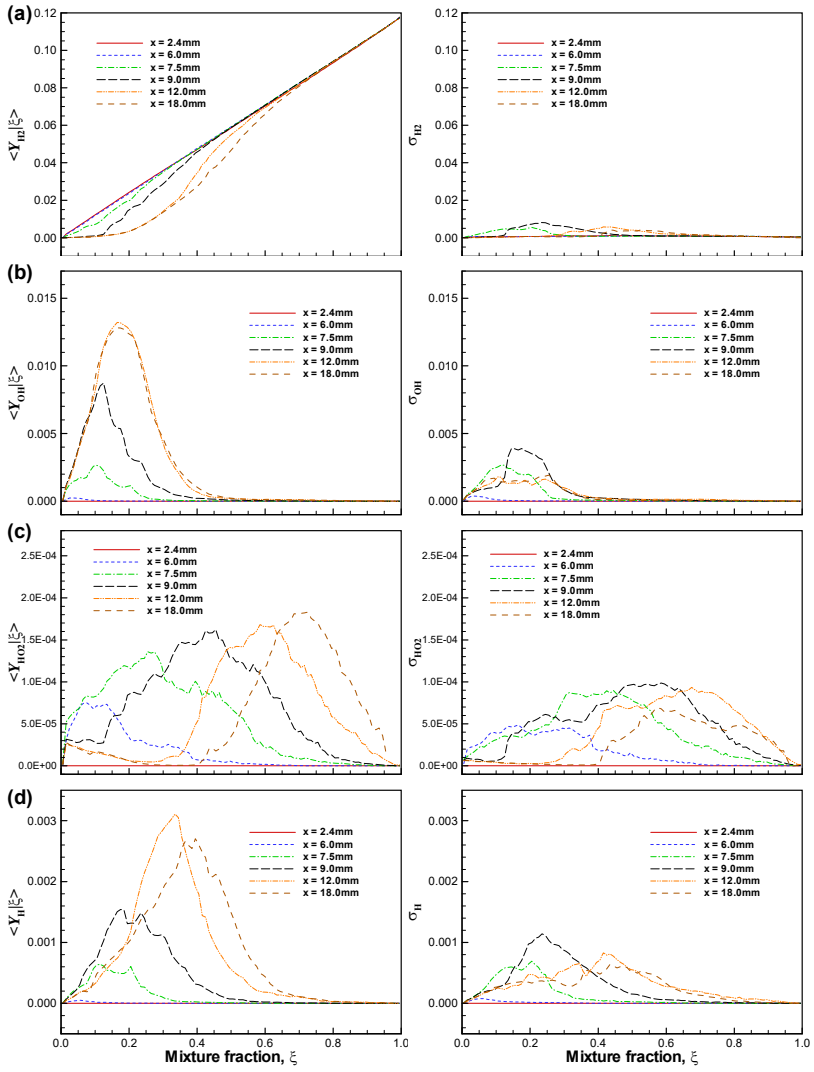

Figure 10: Conditional means and standard deviations of (a) Y_{H2}, (b) Y_{OH}, (c) Y_{HO2}, and (d) Y_{H} for different axial locations at t = 0.42ms.

These flame characteristics can also be found in the behavior of the important species mass fractions and reaction rates. Figures 10 and 11 show the conditional means and standard deviations of H_2, OH, HO_2 and H species mass fraction and their reaction rates, respectively. One can readily observe that the peak reaction rates of each intermediate species spatially precede the peaks of the corresponding species, and thus, HO_2 radical builds up at x = 6mm ahead of OH and H radicals. In the same context, the peaks of HO_2 and H radicals move toward richer mixtures at downstream axial positions because HO_2 is produced in a low temperature region, and H radical is generated under fuel rich conditions in a flame, and thus, the peaks of the species follow the core jet of cold fuel. However, the peak of OH radical occurs near the stoichiometric mixture after x = 12mm, which coincides with the peak temperature region. It is of interest to note that the fuel consumption rate exhibits two peaks

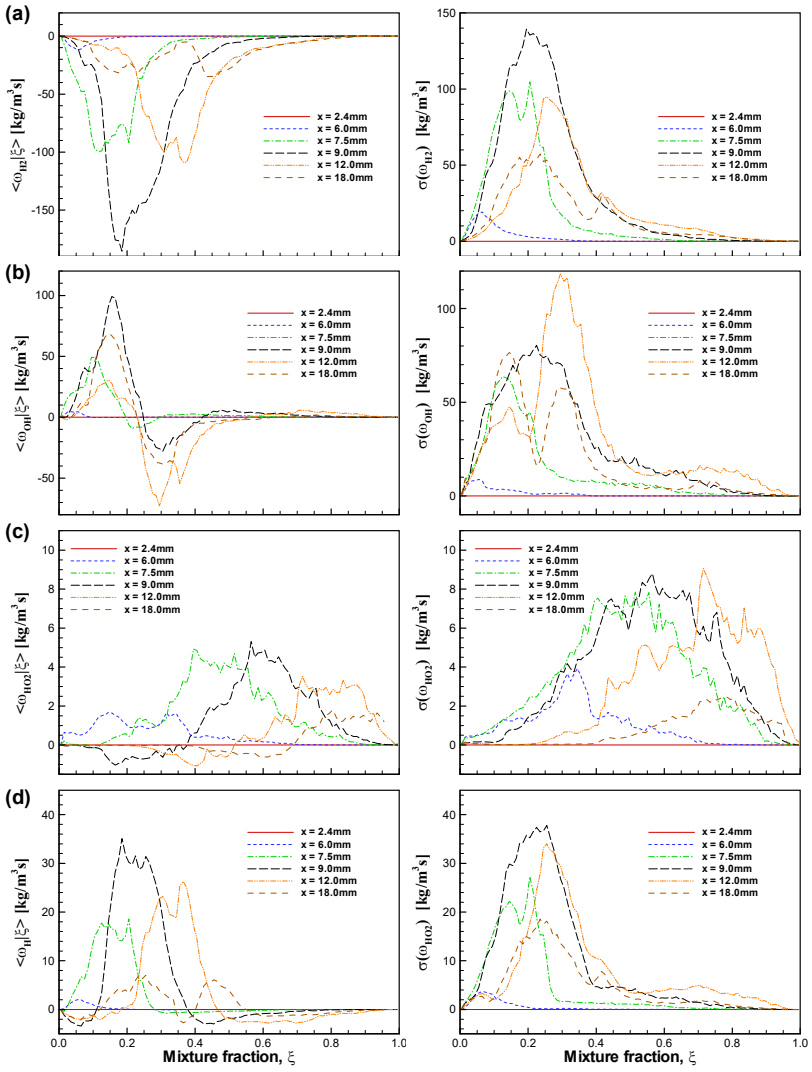

Figure 11: Conditional means and standard deviations of the reaction rates of (a) H_2, (b) OH, (c) HO_2, and (d) H for different axial locations at t = 0.42ms.

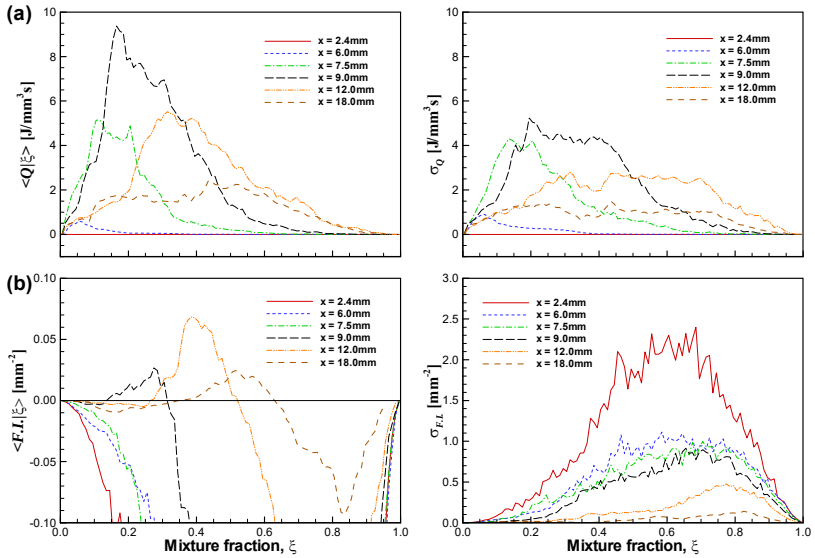

Figure 12: Conditional means and standard deviations of (a) heat release rate and (b) flame index for different axial locations at t = 0.42ms.

at x = 18mm, corresponding to stoichiometric and rich mixtures, which clearly coincides with the dual existence of nonpremixed and rich premixed flame modes discussed in section 3.2. Note also that, in general, the conditional standard deviations of the mass fractions and reaction rates exhibit their spatial peaks at x = 9mm, which implies that vigorous reaction and heat release occur at that position, and hence, generate such large conditional deviations.

The conditional means and standard deviations of heat release rate and flame index are presented in Fig. 12. The transition of reactions from lean to rich mixtures is also found in the conditional mean of heat release rate. Finally, twin peaks in the heat release rate form further downstream of the flame base as seen in the fuel consumption rate. It is also of interest to note that near the flame base, the conditional mean of the flame index indicates that the nonpremixed flame mode prevails in a lean mixture where the primary heat release occurs. However, the existence of both premixed and nonpremixed flame modes in the region is observed as shown in Fig. 7 and thus, it is suspected that large magnitudes of the nonpremixed flame index compared to the premixed flame may skew the bias of the conditional mean in lean mixtures. This flame index characteristic can be observed in the conditional standard deviation: *i.e.* upstream of the flame base, large standard deviations exist compared to downstream values. However, at x = 9 and 12mm, the premixed flame mode prevails in stoichiometric and rich mixtures with large heat release rate. Further downstream, nonpremixed flame mode near stoichiometric mixtures and premixed flame mode in fuel-rich mixtures prevail, consistent with the previous discussion.

To determine the relative importance of turbulent mixing with auto-ignition on the stabilization mechanism, the scalar dissipation rate, χ and the Damköhler number, Da are computed to isolate each effect. While the build-up of HO_2 upstream of other intermediate species (H, OH, and O) in the present lifted flame provides evidence of auto-ignition at the

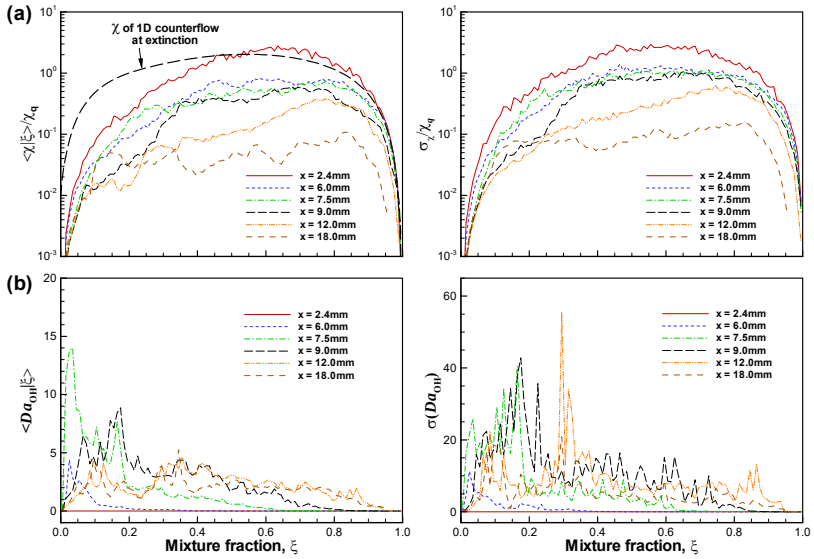

Figure 13: Conditional means and standard deviations of (a) scalar dissipation rate and (b) Da_{OH} for different axial locations at t = 0.42ms.

flame base[23], Da based on species reaction and diffusion terms provides quantitative information regarding the progress of ignition. Significant losses of heat and radicals due to scalar dissipation rate can impede or cause ignition progress slow down or cease[37] as manifested in a Da~ O(<1). In this study, OH radical is chosen to evaluate Da since its exponential growth through chain branching at the expense of a near constant dissipative loss, provides independent evidence of ignition. Da is defined as[37]:

$$Da_k = \frac{\dot{\omega}_k}{-\partial / \partial x_j (\rho Y_k V_{j,k})}, \tag{4}$$

where the subscript k denotes the k-th species with a mass fraction, Y_k, a diffusive velocity in the j direction, $V_{j,k,}$ and a net production rate, $\dot{\omega}_k$.

The conditional means and standard deviations of scalar dissipation rate and Damköhler number based on OH, Da_{OH} are presented in Fig. 13. It is of interest to note that the conditional mean of scalar dissipation rate is substantially below the extinction scalar dissipation rate, χ_q (≈ 10400s^{-1} at ξ_{st}) of a strained laminar nonpremixed flame, even near the fuel jet nozzle, and it becomes an order of magnitude smaller than χ_q near the flame base. The χ_q is evaluated using OPPDIF[38] at the extinction point. This result implies that the nonpremixed flamelet theory, which conjectures that a lifted flame stabilizes where the local scalar dissipation rate decreases below a critical value, or the extinction scalar dissipation rate, is not the mechanism by which the flame stabilizes. This problem with the nonpremixed flame theory was previously reported[3, 39].

Rather, the conditional mean of Da_{OH} as shown in Fig. 13 (b) clearly shows that auto-ignition is the main source of stabilization of the lifted flame, since Da_{OH} of a lean mixture at the flame base is of order ten, and not unity as it would be in a flame. Further downstream,

Da_{OH} approaches unity throughout the entire mixture, which indicates a transition from auto-ignition to premixed or nonpremixed flames where reaction balances diffusion. However, we still see large standard deviation downstream of the flame base (x = 12mm). This result implies that there still exists local auto-ignition in fuel-rich mixtures with large Damköhler number. In addition to the Damköhler number analysis, the speed of flame base also indicates auto-ignition. Note that before the flame base attains a steady-state, it propagates upstream at approximately 60m/s in the laboratory reference frame. This flame speed is much larger than the laminar flame speed corresponding to the stoichiometric mixture in the present study at high temperature (e.g. $s_L \sim 11.6$m/s at 800K) [40], which implies that the flame base is not a deflagration wave but a spontaneous subsonic ignition front[41].

3.4 Vortex generation near flame base

As seen earlier in Figs. (4) and (5), a vortex exists near the flame base which helps the base stabilize. In this section, the vorticity generation/attenuation mechanism near the flame base is investigated. Vorticity is usually generated or attenuated by several different mechanisms and thus, the vorticity balance equation provides the contributions of each mechanism to the enhancement or attenuation of vorticity. For compressible flows, the vorticity transport equation is given by[36]:

$$\frac{D\boldsymbol{\omega}}{Dt} = (\boldsymbol{\omega}\cdot\nabla)\mathbf{u} - \boldsymbol{\omega}(\nabla\cdot\mathbf{u}) + \nu\nabla^2\boldsymbol{\omega} + \frac{1}{\rho^2}(\nabla\rho\times\nabla p), \tag{5}$$

where $\boldsymbol{\omega}$ and $\mathbf{u}$ are the vorticity and velocity vectors, respectively, with the kinematic viscosity, ν, the mass density, ρ and the pressure, p. The first term on the r.h.s. of Eq. (5) is the vortex stretching term which accounts for the vortex straining by the local flow, and the second term corresponds to vorticity attenuation by flow dilatation due to heat release. The third and fourth terms represent vorticity attenuation and generation by diffusion and baroclinic torque, respectively. Equation (5) does not include viscosity gradients which, in general, are negligible in flames[32].

The contributions to vorticity generation by vortex stretching and diffusion are significant in the highly turbulent central fuel jet core. In the present configuration of a lifted jet flame in a heated coflow, the flame base lies in a lean mixture outside of the fuel jet, as previously discussed, and thus, the main vorticity attenuation and generation near the flame base is due to baroclinic torque. Vorticity attenuation by flow expansion is also negligible outside of the flame.

Figure 14 shows a schematic of spanwise vorticity generation (sign convention is vorticity is positive coming out of the paper) near the flame base by baroclinic torque. In this particular lifted flame, density in the mixing layer is lower than in the heated coflow and in the cold fuel jet. This is because density in the mixing layer is affected not only by local temperature but also by the local mixture molecular weight which monotonically increases from the fuel jet to the hot oxidizer, and hence, density exhibits its local minimum in the mixing layer. Therefore, near the right branch of the flame base the gradient of density is in the direction towards the heated coflow. However, the gradient of pressure is in the direction

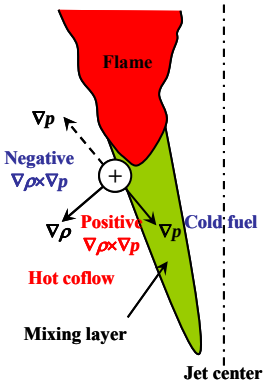

Figure 14: Schematic of spanwise vorticity generation by baroclinic torque.

of the cold fuel jet or the hot coflow as shown in Fig. 14. Therefore, the misalignment of the two gradients ($\nabla\rho \times \nabla p$) yields vorticity generation/attenuation depending on the local pressure field.

Figure 15 shows the isocontours of the spanwise vorticity generation by baroclinic torque normalized by the local magnitude of total vorticity generation. One can readily deduce that, compared to the central core jet region, the dominant vorticity generation mechanism outside of the flame is by baroclinic torque. By examining Figs. 4 and 15, one can see that the vorticity generation produces a positive vortex near the flame base right after the extinction. Thus, one may conclude that the vorticity generation by the baroclinic torque can assist the stabilization of the flame base by reducing the local incoming velocity. The origin of the baroclinic torque is a subject of ongoing investigation. In particular, the source of the pressure gradient – due to acoustic generation or due to vortices – in the mixing layer needs to be clarified.

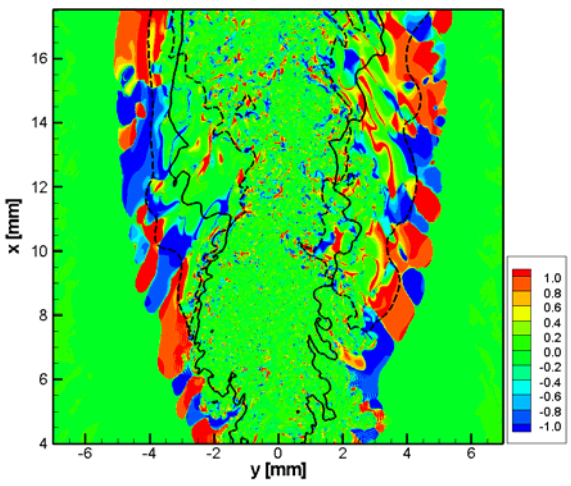

Figure 15: Spanwise vorticity generation by baroclinic torque normalized by the local magnitude of total vorticity generation in the $z = 0$ plane at $t = 0.42$ms. Solid and dashed lines represent stoichiometric mixture fraction, ξ_{st} and Y_{OH} isocontour of 0.001, respectively.

4 CONCLUDING REMARKS

Three-dimensional direct numerical simulation of a turbulent lifted hydrogen/air jet flame in an auto-ignitive heated coflow was performed using detailed chemistry and mixture-averaged transport properties. The results show that auto-ignition is the key mechanism responsible for flame stabilization, and HO_2 radical is important in initiating the auto-ignition ahead of the flame base. Nominally, auto-ignition is found to occur in hot, fuel-lean regions, but occasionally it occurs in a fuel-rich mixture after local flame extinction or in a fuel-rich island issuing from the central core fuel jet. The Damköhler number analysis and the spatial behavior of the intermediate species clearly demonstrate the presence of auto-ignition at the flame base: *i.e.* large values of Da_{OH} near the flame base indicates auto-ignition and the existence of HO_2 upstream of high-temperature radicals, O, OH, and H, also is a hallmark of auto-ignition.

From the flame index at the flame base, it was found that both fuel-lean premixed and nonpremixed flame modes exist. However, the premixed flame mode prevails downstream of the flame base and finally, both rich premixed and nonpremixed flame modes develop further downstream. The conditional mean of the scalar dissipation rate is found to be an order of magnitude smaller than the laminar extinction scalar dissipation rate at the flame base, implying that the nonpremixed flamelet theory does not provide a stabilization mechanism.

Assisting auto-ignition as the primary stabilization mechanism, vorticity generation near the flame base due to the baroclinic torque seemed to adjust the strength of incoming vortices in a manner that reduces the local axial velocity, and hence, provides a sheltered environment for auto-ignition to proceed.

ACKNOWLEDGEMENTS

The work at Sandia National Laboratories (SNL) was supported by the Division of Chemical Sciences, Geosciences, and Biosciences, Office of Basic Energy Sciences of the U. S. Department of Energy, and the U. S. Department of Energy SciDAC Program. SNL is a multiprogram laboratory operated by Sandia Corporation, a Lockheed Martin Company, for the U. S. Department of Energy under contract DE-AC04-94AL85000. The work at Oak Ridge National Laboratory (ORNL) was supported by and this research used resources of the National Center for Computational Sciences (NCCS) at ORNL, which is supported by the Office of Science of the U.S. DOE under contract DE-AC05-00OR22725.

REFERENCES

[1] K. M. Lyons, “Toward an understanding of the stabilization mechanisms of lifted turbulent jet flames: Experiments”, *Prog. Energy Combust. Sci*., **33**, 211–231 (2007).

[2] W. M. Pitts, “Assessment of theories for the behavior and blowout of lifted turbulent jet diffusion flames”, *Proc. Combust. Inst*., **22**, 809–816 (1988).

[3] N. Peters, *Turbulent combustion*, Cambridge University Press, New York, (2000).

[4] L. Vanquickenborne and van A. Tiggelen, “The stability mechanism of lifted diffusion flames”, *Combust. Flame*, **10**, 59–69 (1966).

[5] G. T. Kalghatgi, "Lift-off heights and visible lengths of vertical turbulent jet diffusion flames in still air", *Combust. Sci. Technol*., **41**, 17–29 (1984).
[6] N. Peters and F. A. Williams, "Liftoff characteristics of turbulent jet diffusion flames", *AIAA J*., **21**, 423–429 (1983).
[7] A. Upatnieks, J. F. Driscoll, C. C. Rasmussen, and S. L. Ceccio, "Liftoff of turbulent jet flames–assessment of edge flame and other concepts using cinema-PIV", *Combust. Flame*, **138**, 259–272 (2004).
[8] A. Joedicke, N. Peters, and M. Mansour, "The stabilization mechanism and structure of turbulent hydrocarbon lifted flames", *Proc. Combust. Inst*., **30**, 901–909 (2005).
[9] H. Phillips, "Flame in a buoyant methane layer", *Proc. Combust. Inst*., **10**, 1277–1283 (1965).
[10] S. H. Chung, "Stabilization, propagation and instability of tribrachial triple flame", *Proc. Combust. Inst*., **31**, 877–892 (2007).
[12] M. M. Tacke, D. Geyer, E. P. Hassel, and J. Janicka, "A detailed investigation of the stabilization point of lifted turbulent diffusion flames", *Proc. Combust. Inst*., **27**, 1157–1165 (1998).
[12] L. K. Su, O. S. Sun, and M. G. Mungal, "Experimental investigation of stabilization mechanisms in turbulent, lifted jet diffusion flames", *Combust. Flame*, **144**, 494–512 (2006).
[13] J. B. Kelman, A. J. Eltobaji, and A. S. Maris, "Laser imaging in the stabilization region of turbulent lifted flames", *Combust. Sci. Technol.*, **135**, 117–134 (1998).
[14] R. Cabra, T. Myhrvold, J. Y. Chen, R. W. Dibble, A. N. Karpetis, and R. S. Barlow, "Simultaneous laser Raman-Rayleigh-LIF measurements and numerical modeling results of a lifted turbulent H_2/N_2 jet flame in a vitiated coflow", *Proc. Combust. Inst*., **29**, 901–909 (2002).
[15] C. N. Markides and E. Mastorakos, "An experimental study of hydrogen autoignition in a turbulent co-flow of heated air", *Proc. Combust. Inst*., **30** , 883–891 (2005).
[16] L. M. Pickett, "Low flame temperature limits for mixing-controlled Diesel combustion", *Proc. Combust. Inst*., **30**, 2727–2735 (2005).
[17] H. Yamashita, M. Shimada, and T. Takeno, "A numerical study on flame stability at the transition point of jet diffusion flames", *Proc. Combust. Inst*., **26**, 27–34 (1996).
[18] C. Jiménez and B. Cuenot, "DNS study of stabilization of turbulent triple flames by hot gases", *Proc. Combust. Inst*., **31**, 1649–1656 (2007).
[19] Y. Mizobuchi, S. Tachibana, J. Shinio, and S. Ogawa, "A numerical analysis of the structure of a turbulent hydrogen jet lifted flame", *Proc. Combust. Inst*., **29**, 2009–2015 (2002).
[20] Y. Mizobuchi, S. Tachibana, J. Shinio, and S. Ogawa, "A numerical study on the formation of diffusion flame islands in a turbulent hydrogen jet lifted flame", *Proc. Combust. Inst*., **30**, 611–619, (2005).
[21] A. R. Masri, R. Cao. S. B. Pope, and G. M. Goldin, "PDF calculations of turbulent lifted flames of H2/N2 fuel issuing into a vitiated co-flow", *Combust. Theory Modelling*, **8**, 1–22 (2004).

[22] R. R. Cao, S. B. Pope, A. R. Masri, "Turbulent lifted flames in a vitiated coflow investigated using joint PDF calculations", *Combust. Flame*, **142**, 438–453 (2005).
[23] R. L. Gordon, A. R. Masri, S. B. Pope, and G. M. Goldin, "A numerical study of auto-ignition in turbulent lifted flames issuing into a vitiated co-flow", *Combust. Theory Modelling*, **11**, 351-376 (2007).
[24] K. Gkagkas and R. P. Lindstedt, "PDF modeling of hydrogen/air lifted flame", *8th International Workshop on measurement and computation of turbulent nonpremixed flames*, Heidelberg, Germany, Aug. 3-5 (2006).
[25] C. K. Law, *Combustion Physics*, Cambridge University Press, New York, p89–93 (2006)
[26] R. Sankaran, E. R. Hawkes, J. H. Chen, T. Lu, and C. K. Law, "Structure of a spatially developing turbulent lean methane-air Bunsen flame", *Proc. Combust. Inst*., **31**, 1291–1298 (2007).
[27] C. A. Kennedy and M. H. Carpenter, "Several new numerical methods for compressible shear-layer simulations", *Appl. Num. Math.*, **14**, 397–433 (1994).
[28] C. A. Kennedy, M. H. Carpenter, and R. M. Lewis, "Low-storage, explicit Runge-Kutta schemes for the compressible Navier-Stokes equations", *Appl. Num. Math*., **35**, 177–264 (2000).
[29] J. Li, Z. Zhao, A. Kazakov, and F. Dryer, "An updated comprehensive kinetic model of hydrogen combustion", *Int. J. Chem. Kinet.*, **36**, 566–575 (2004).
[30] R. J. Kee, F. M. Rupley, E. Meeks, and J. A. Miller, *CHEMKIN-III: A Fortran Chemical Kinetics Package for the Analysis of Gas-Phase Chemical and Plasma Kinetics*, Report No. SAND96-8216, Sandia National Laboratories, (1996).
[31] R. J. Kee, G. Dixon-Lewis, J. Warnatz, M. E. Coltrin, and J. A. Miller, *A Fortran Computer Code Package for the Evaluation of Gas-Phase Multicomponent Transport Properties*, Report No. SAND86-8246, Sandia National Laboratories, (1986).
[32] C. S. Yoo, Y. Wang, A. Trouvé, and H. G. Im, "Characteristic boundary conditions for direct simulations of turbulent counterflow flames", *Combust. Theory Modelling*, **9**, 617–646 (2005).
[33] C. S. Yoo and H. G. Im, "Characteristic boundary conditions for simulations of compressible reacting flows with multi-dimensional, viscous and reaction effects", *Combust. Theory Modelling*, **11**, 259–286 (2007).
[34] R. W. Schefer and P. J. Goix, "Mechanism of flame stabilization in turbulent, lifted-jet flames", *Combust. Flame*, **112**, 559–574 (1998).
[35] R. W. Bilger, "The structure of turbulent nonpremixed flames", *Combust. Flame*, **22**, 475–488 (1988).
[36] C. J. Mueller, J. F. Driscoll, D. L. Reuss, M. C. Drake, and M. E. Rosalik, "Vorticity generation and attenuation as vortices convect through a premixed flame", *Combust. Flame*, **112**, 342–358 (1998).
[37] T. Echekki and J. H. Chen, "Direct numerical simulation of autoignition in nonhomogeneous hydrogen-air mixtures", *Combust. Flame*, **134**, 161–191 (2003).
[38] A. E. Lutz, R. J. Kee, J. F. Grcar, F. M. Rupley, *OPPDIF: A Fortran Program for Computing Opposed–Flow Diffusion Flames*, Report No. SAND96-8243, Sandia

National Laboratories, (1997).
[39] E. F. Hasselbrink and M. G. Mungal, "Characteristics of the velocity field near the instantaneous base of lifted non-premixed turbulent jet flames", *Proc. Combust. Inst*., **27**, 867–873 (1998).
[40] R. J. Kee, J. F. Grcar, M. D. Smooke, and J. A. Miller, *Fortran program for modeling steady laminar one-dimensional premixed flames*, Report No. SAND85-8240, Sandia National Laboratories, (1985).
[41] Y. B. Zeldovich, "Regime classification of an exothermic reaction with nonuniform initial conditions", *Combust. Flame*, **39**, 211–214 (1980).